J. IMBROCK[1],✉
C. BÄUMER[1]
H. HESSE[1]
D. KIP[2]
E. KRÄTZIG[1]

Photorefractive properties of iron-doped lithium tantalate crystals

[1] University of Osnabrück, Physics Department, 49069 Osnabrück, Germany
[2] Technical University of Clausthal, Institute of Physics, 38678 Clausthal-Zellerfeld, Germany

ABSTRACT Iron-doped lithium tantalate crystals are grown by the Czochralski method and their photorefractive properties are examined with holographic methods. Dynamic range, holographic sensitivity, photoconductivity, and dark storage time are measured in dependence on the iron concentration and light intensity. The largest refractive-index change for ordinarily polarized light is 3.5×10^{-4}, in comparison with 6.2×10^{-4} for iron-doped lithium niobate. Due to a small mobility of protons the dark storage time of holograms in lithium tantalate is larger than that in lithium niobate.

PACS 42.40.Pa; 42.70.Ln

1 Introduction

Photorefractive crystals like lithium niobate ($LiNbO_3$) and lithium tantalate ($LiTaO_3$) are promising materials for applications such as holographic data storage [1] and filters for wavelength-division multiplexers [2]. $LiNbO_3$ and $LiTaO_3$ exhibit large dark storage times and nondestructive read out of holograms can be realized using different methods, e.g. thermal or optical fixing. The photorefractive properties of $LiNbO_3$ have been examined in detail in the past, especially by using holographic methods. Holograms can be stored in $LiNbO_3$ by illuminating a crystal with an interference pattern. Electrons are excited from impurities, e.g., Fe^{2+}, to the conduction band. The electrons are redistributed because of drift in an electrical field, diffusion, or the bulk photovoltaic effect. Finally, they are trapped in empty centers, e.g., Fe^{3+}, and the concentration of defects is modulated. A space-charge field builds up that modulates the refractive index through the electro-optic effect. It is known that the photorefractive effect in $LiNbO_3$ can be enhanced by doping the crystal with Fe, Cu, or Mn. The dynamic range, photoconductivity, and sensitivity of iron-doped lithium niobate ($LiNbO_3$: Fe) can be optimized for holographic data storage by varying the doping level of iron and by thermal treatments where iron is reduced or oxidized. However, the dynamic range of $LiNbO_3$: Fe is limited. The dynamic range increases with increasing concentration of Fe^{3+} ions, but for concentrations larger than $c_{Fe^{3+}} \approx 200 \times 10^{23}$ m^{-3} the light-induced refractive-index change saturates [3]. The reason for this is that for large iron concentrations c_{Fe} the specific photoconductivity increases with increasing c_{Fe}. Furthermore, the dark conductivity of highly doped $LiNbO_3$: Fe is very high and the dark storage time can be less than several minutes [4].

$LiTaO_3$ is isomorphous to $LiNbO_3$, but the photorefractive properties of doped $LiTaO_3$ are less examined. Holographic experiments with iron-doped [5, 6] and rhodium-doped [7] congruently melting $LiTaO_3$ crystals have been performed using continuous-wave (cw) laser light, but a detailed investigation of the performance of $LiTaO_3$ as a holographic storage material is still missing. One reason for this might be that $LiTaO_3$ is more difficult to grow due to its higher melting point of about 1650 °C [8]. A further reason is a larger band gap of $LiTaO_3$ compared to $LiNbO_3$ (4.6 eV versus 3.7 eV) and therefore the spectral sensitivity of doped $LiTaO_3$ is shifted to the ultraviolet region. $LiNbO_3$: Fe for instance is most sensitive around 480 nm, while $LiTaO_3$: Fe has its absorption maximum at 400 nm. With the invention of compact high-power laser sources in the ultraviolet, $LiTaO_3$: Fe might become an alternative to $LiNbO_3$: Fe for several applications. Here the question arises whether $LiTaO_3$: Fe shows the same limits as $LiNbO_3$: Fe concerning the dynamic range. Another important parameter for holographic data-storage applications is the dark storage time. The dark storage time of holograms in moderately doped $LiNbO_3$: Fe at room temperature is about one year. It is expected that the dark storage time of $LiTaO_3$ considerably exceeds that of $LiNbO_3$ [5].

We have examined the photorefractive properties of $LiTaO_3$: Fe with both holographic and conventional methods. For this purpose we have grown iron-doped $LiTaO_3$ crystals of five different iron concentrations using the Czochralski method. The dynamic range, bulk photovoltaic current, holographic sensitivity, photoconductivity, and dark conductivity are measured. The values obtained are compared with typical values for $LiNbO_3$.

2 Fundamentals

During illumination of a $LiTaO_3$: Fe crystal with two intersecting coherent laser beams, electrons are excited from Fe^{2+} ions and migrate in the conduction band before

✉ Fax: +49-541/969-3510, E-mail: joerg.imbrock@uos.de

they are finally trapped in Fe^{3+} ions. Intrinsic defects like Ta ions at Li sites are not considered here. At moderate continuous-wave laser intensities ($I < 10 \, kW/m^2$) these antisite defects do not contribute to the light-induced charge transport. However, at higher light intensities or in specially treated crystals the intrinsic defects have to be considered as a second photorefractive center [6, 9]. The modulated concentration of iron ions finally leads to a space-charge field. This space-charge field E_{SC} modulates the refractive index $n_{o,e}$ for ordinarily and extraordinarily polarized light through the electro-optic effect:

$$\Delta n_{o,e} = -\frac{1}{2} n_{o,e}^3 r_{13,33} E_{SC} \,. \tag{1}$$

Here $r_{13,33}$ denote the electro-optic coefficients for ordinarily and extraordinarily polarized light, respectively. Values of $n_{o,e}$ and $r_{13,33}$ are given in Table 1 for $LiTaO_3$ and $LiNbO_3$. To calculate the space-charge field the corresponding rate equation describing the charge transport with one photorefractive center has to be solved considering the continuity equation and the Poisson equation. Solutions for the time development of the space-charge field are given by Kukhtarev et al. [10]. In iron-doped $LiNbO_3$ and $LiTaO_3$ the current density j is mainly determined by the bulk photovoltaic current density j_{phv} [11], which is proportional to the light intensity I and the concentration of filled centers $c_{Fe^{2+}}$:

$$j \approx j_{phv} \propto \beta^* I c_{Fe^{2+}} \,. \tag{2}$$

Here β^* denotes the specific photovoltaic coefficient. The photoconductivity σ_{ph} increases linearly with increasing light intensity I and increasing $c_{Fe^{2+}}/c_{Fe^{3+}}$ concentration ratio [12]:

$$\sigma_{ph} \propto I \frac{c_{Fe^{2+}}}{c_{Fe^{3+}}} \,. \tag{3}$$

Therefore, the specific photoconductivity

$$f = \left(\frac{\sigma_{ph}}{I} \right) \Big/ \left(\frac{c_{Fe^{2+}}}{c_{Fe^{3+}}} \right) \tag{4}$$

should be constant and should not depend, for example, on the total iron concentration c_{Fe}. The current density j_{phv} (2) and the photoconductivity σ_{ph} (3) yield the steady state space-charge field $E_{SC} = j_{phv}/\sigma_{ph}$. Hence, the saturation value of the refractive-index change Δn_S is proportional to the concentration of Fe^{3+} (1):

$$\Delta n_S \propto c_{Fe^{3+}} \,. \tag{5}$$

The dark storage time τ_d is determined by the dark conductivity σ_d. If the iron concentration is not too high, σ_d mainly depends on the concentration of protons c_p, because in the dark protons are mobile and compensate for the space-charge field:

$$\sigma_d = e \mu_p c_p \,. \tag{6}$$

Here e is the elementary charge, μ_p the mobility of the protons, and c_p the concentration of the protons. The proton concentration depends linearly on the absorption coefficient of the OH^- stretching vibration at 2870 nm for ordinarily polarized light ($c_p \propto \alpha_{2870 \, nm}^o$) [13]. The temperature dependence of the dark storage time can often be described by an Arrhenius law:

$$\tau_d = \varepsilon \varepsilon_0 / \sigma_d \propto \exp[E_A/(k_B T)] \,, \tag{7}$$

with the dielectric constant ε ($LiNbO_3 : \varepsilon_{33} = 28$; $LiTaO_3 : \varepsilon_{33} = 43$), the permittivity of free space ε_0, the temperature T, the Boltzmann constant k_B, and the activation energy E_A. The activation energy of protons in $LiNbO_3 : Fe$ varies with proton concentration, iron concentration, and temperature between 1.0 eV and 1.2 eV [14–16].

3   Experimental methods

3.1   *Crystal growth and preparation*

Iron-doped congruently melting $LiTaO_3$ crystals are grown by the Czochralski technique using a resistance-heating furnace. With this furnace a maximum temperature of about 1720 °C (the melting point of $LiTaO_3$ is about 1650 °C [8]) can be achieved. The temperature gradient above the melt is smaller than 10 °C and air is used as growth atmosphere. For the growth a platinum crucible is used. The starting material is pure (99.998%) $LiTaO_3$; Li_2O losses in the growth experiments are compensated with Li_2CO_3 (99.999%). Iron doping is realized by giving Fe_2O_3 to the melt. A seed rotation rate of 20 rpm and a pulling rate of 0.5 mm/h are applied. A crystal boule has a typical size of 15 mm in diameter and a height of 25 mm. The weight is about 30 g. We have grown pure crystals ('LT16') and five crystals with iron concentrations between 0.01 wt. % and 0.08 wt. % Fe (Table 2).

After the growth process the crystals are orientated and cut into pieces with a typical size of $x \times y \times z = 4 \times 1 \times 5 \, mm^3$. Each sample is polished to optical quality. The Fe^{2+}/Fe^{3+}

LiTaO_3	c_{Fe}^{melt} [10^{23} m^{-3}]	$c_{Fe}^{crystal}$ [10^{23} m^{-3}]
LT16	–	10
LT17	80	110
LT18	160	190
LT19	320	350
LT20	480	510
LT21	640	670

TABLE 2 $LiTaO_3$ crystals grown by the Czochralski method and their contents of iron. The concentrations in the second column are the concentrations of Fe that were given to the melt, and the concentrations in the third column are determined by the absorption spectra [5, 6]. The crystal 'LT16' is undoped

Coefficient	LiTaO_3	LiNbO_3
n_o	2.177	2.286
n_e	2.181	2.203
r_{13}	8.4 pm/V	10.9 pm/V
r_{33}	30.5 pm/V	34.0 pm/V

TABLE 1 Refractive indices $n_{o,e}$ [22, 23] and electro-optic coefficients $r_{13,33}$ [24] for ordinarily and extraordinarily polarized light (wavelength $\lambda = 633$ nm) of congruently melting $LiTaO_3$ and $LiNbO_3$

concentration ratio ($c_{Fe^{2+}}/c_{Fe^{3+}}$) can be varied by different annealing treatments. Heating a $LiTaO_3$ crystal in an argon atmosphere or in vacuum to temperatures of about 1000 °C increases the $c_{Fe^{2+}}/c_{Fe^{3+}}$ concentration ratio. Large concentration ratios ($c_{Fe^{2+}}/c_{Fe^{3+}} > 1$) are only achieved using vacuum with an air pressure less than 10^{-2} mbar. Heating a crystal in an oxygen atmosphere oxidizes the iron ions ($c_{Fe^{2+}}/c_{Fe^{3+}} < 0.1$). After the growth process and after thermal treatments the crystals have to be poled. This is done by heating them above the Curie temperature to 700 °C. Then, an electric field of about 30 V/cm is applied parallel to the c axis while cooling. To test whether a crystal is completely poled, the piezo-electric effect is measured. The piezo-electric coefficient of a completely poled crystal is about 7.8 pC/N [17].

To determine the concentrations of Fe^{2+} and Fe^{3+} the absorption coefficients of the crystals are measured with a CARY 17D spectrometer. The absorption coefficients for ordinarily polarized light at 400 nm ($\alpha^o_{400\,nm}$) and 310 nm ($\alpha^o_{310\,nm}$) yield the concentrations $c_{Fe^{2+}}$ and $c_{Fe^{3+}}$ [5, 6]:

$$c_{Fe^{2+}} = 2.13 \times 10^{21}\ \mathrm{m}^{-2}\,\alpha^o_{400\,nm}\,, \tag{8}$$

$$c_{Fe^{3+}} = 5.33 \times 10^{20}\ \mathrm{m}^{-2}\,\alpha^o_{310\,nm}\,. \tag{9}$$

The total iron concentrations of the six crystals determined from the absorption spectra are also given in Table 2. These concentrations are slightly higher than the content of Fe that was given to the melt.

3.2 *Holographic characterization*

A two-beam interference setup is used to record holograms in the $LiTaO_3$: Fe crystals (see Fig. 1). Ordinarily polarized light of an Ar-ion laser is expanded and split into two beams (R1 and R2) of equal intensity. These beams are superimposed inside the crystal and the vector $\boldsymbol{K}$ of the light grating is parallel to the crystal's c axis. The grating
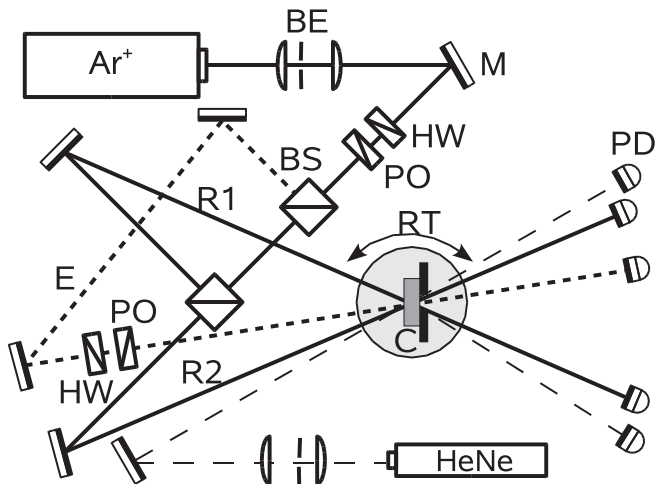

FIGURE 1 Schematic drawing of the holographic setup. Two ordinarily polarized recording beams (R1 and R2) of an Ar-ion laser are superimposed inside the crystal (C). During hologram recording and erasure, the grating can be probed with red light ($\lambda = 633$ nm, ordinarily polarized) of a He–Ne laser. Off-Bragg erasure is achieved by illuminating the crystal with a different beam (E). BE: beam expander, M: mirror, HW: $\lambda/2$ plate, PO: polarizer, BS: beam splitter, RT: rotary table, PD: photodiode

period $\Lambda = 2\,\pi/K$ is about 0.8 μm. The crystal is mounted on a rotary stage and it is placed in front of an aperture with a diameter of 1 mm. The transmitted light of the recording beams is detected with photodiodes. To erase a hologram off-Bragg, the crystal can be illuminated homogeneously with a third beam (E). This beam can also be used during hologram recording to reduce the modulation of the interference pattern, because the difference in the path lengths of the beams R and E is larger than the coherence length of the laser. The intensities of the beams can be varied by means of a combination of a $\lambda/2$ plate and a polarizer. During hologram recording and erasure, a hologram can be probed with a weak beam of a He–Ne laser ($\lambda = 633$ nm), which is ordinarily polarized and Bragg matched. The diffracted and transmitted beams of the probe laser are detected with photodiodes that are provided with interference filters to block scattered light of the Ar-ion laser. While recording a hologram, the transmitted intensity I_t and the diffracted intensity I_d of the probe-laser beam are measured. These intensities yield the diffraction efficiency $\eta = I_d/(I_d + I_t)$. Using Kogelnik's formula [18]

$$\eta = \sin^2\left(\frac{\pi\,\Delta n\,d}{\lambda\cos\Theta}\right) \tag{10}$$

we calculate the refractive-index change Δn. Here d denotes the crystal thickness, λ the vacuum wavelength, and Θ half of the angle between the recording beams inside the crystal. When the recorded hologram has reached its saturation value of refractive-index change Δn_S, one recording beam is blocked and the hologram is read with the remaining beam. The resulting refractive-index change is compared with that calculated from the diffracted light of the probe laser to ensure a proper alignment of the probe-laser beam. Additionally, we can read a hologram with the He–Ne laser beam and rotate the crystal slightly to check whether the probe-laser beam is correctly Bragg matched. Crystals with different Fe^{2+} concentrations exhibit different absorption constants in the visible. An averaged intensity is calculated using the formula

$$I = I_{in}\frac{1-R}{\alpha^o d}\frac{1-\exp(-\alpha^o d)}{1-R\exp(-\alpha^o d)}\,. \tag{11}$$

Here R denotes the reflectivity, α^o the absorption coefficient at the recording wavelength, and I_{in} the intensity of the incident light.

When a $LiTaO_3$ crystal is illuminated homogeneously a bulk photovoltaic current flows along the c axis. We measure this current by contacting the surfaces perpendicular to the c axis with silver-paste electrodes and connecting the electrodes with a high-sensitivity electrometer. By means of a monochromator the wavelength of a xenon arc lamp can be adjusted between 350 nm and 700 nm. The light is ordinarily polarized and its intensity can be varied with neutral-density filters. To measure the photovoltaic current at larger intensities the light of the Ar-ion laser can also be used.

The dark conductivity of the crystals is determined by measuring the dark decay of a hologram in dependence on the temperature. First, a hologram is recorded to its saturation value of refractive-index change. Then, the crystal is heated to a maximum temperature of 180 °C and the hologram is read every minute by the probe laser. During read out the crystal

is rotated a few degrees and a rocking curve of the diffracted light is measured. After each rocking curve the crystal is rotated automatically to the point of the largest diffraction efficiency. Thus, the hologram is always read under the correct Bragg angle. It is ensured that the light of the probe laser has no influence on the dark decay and the whole setup is put into a box to screen it from daylight. After one dark decay has been measured, the crystal is heated to 180 °C and illuminated with white light to erase all remaining gratings.

4   Experimental results

4.1   Crystals

The grown crystals are free from any cracks or striations. The composition of the crystals can be determined for instance by measuring the temperature of zero birefringence [19], the absorption edge [20], and the Curie temperature T_C because T_C increases with increasing Li content of the crystal. The determined Curie temperature of the investigated crystals is about 600 °C, i.e. they have the congruently melting composition. The absorption coefficient α depends on the amounts of Fe^{2+} and Fe^{3+}. In Fig. 2 an absorption spectrum of two crystals with different iron concentrations can be seen. The crystal 'LT16' is not doped but there is always a small quantity of iron in the starting material. The absorption at 310 nm is attributed to an excitation of electrons from the valence band to Fe^{3+} and the absorption at 400 nm is due to an excitation of electrons from Fe^{2+} to the conduction band [5]. The crystal 'LT18' is doped with 0.02 wt. % Fe and thermally reduced. A reduction in vacuum increases the concentration of Fe^{2+} ions.

4.2   Saturation values of refractive-index changes

The dynamic range increases linearly with increasing trap concentration $c_{Fe^{3+}}$, but for larger concentrations than $250 \times 10^{23}\,\text{m}^{-3}$ the saturation value of refractive-index change Δn_S reaches a maximum of 3.5×10^{-4} (Fig. 3). The

FIGURE 3   Saturation value of refractive-index change Δn_S in dependence on the concentration of Fe^{3+} ions. Up to a concentration of about $250 \times 10^{23}\,\text{m}^{-3}$ Δn_S increases linearly with increasing Fe^{3+} concentration. For larger concentrations Δn_S saturates at a level of 3.5×10^{-4}

value of Δn_S does not depend on the wavelength of the recording light λ_w. Hologram read out with a shorter wavelength than 633 nm yields a slightly larger Δn_S because of a larger refractive index and a larger electro-optic coefficient.

4.3   Bulk photovoltaic effect

The bulk photovoltaic current density j_{phv} along the c axis is proportional to the intensity of the light, but for larger intensities than $10\,\text{kW/m}^2$ the current density j_{phv} increases superlinearly with intensity (Fig. 4). The best fit is achieved with the function $j_{phv} = aI + bI^2$, with the free parameters a and b. For moderate intensities ($I < 10\,\text{kW/m}^2$) the photovoltaic current density can be normalized to the intensity. The normalized photovoltaic current density j_{phv}/I increases linearly with increasing concentration of Fe^{2+} ions.
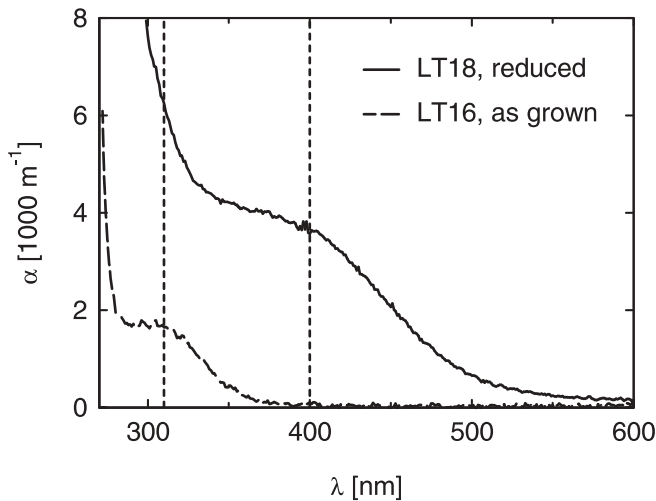
FIGURE 2   Absorption coefficient α versus wavelength λ for ordinarily polarized light. The absorption at 400 nm is proportional to the concentration of Fe^{2+} and the coefficient at 310 nm increases linearly with increasing concentration of Fe^{3+} [5]
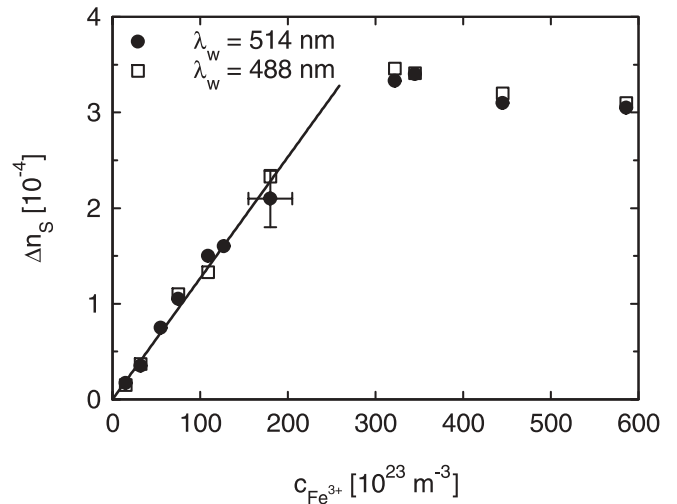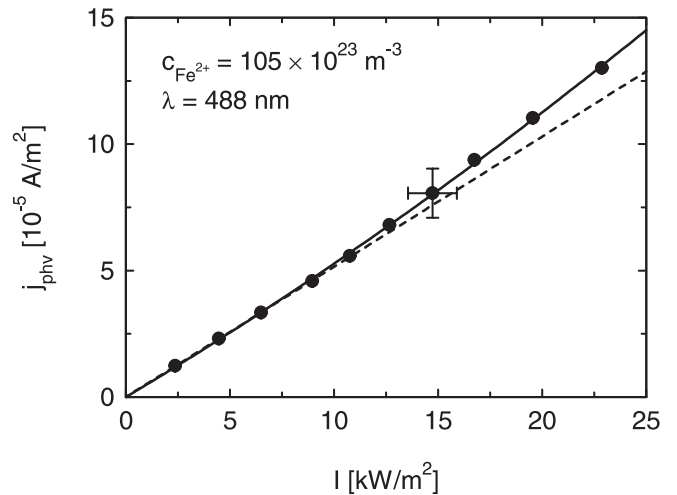
FIGURE 4   Photovoltaic current density j_{phv} along the c axis versus light intensity I. At small intensities j_{phv} increases linearly with increasing intensity (*dashed line*). For larger intensities a superlinear behavior of the form $j_{phv} = aI + bI^2$ is obtained (*solid line*)
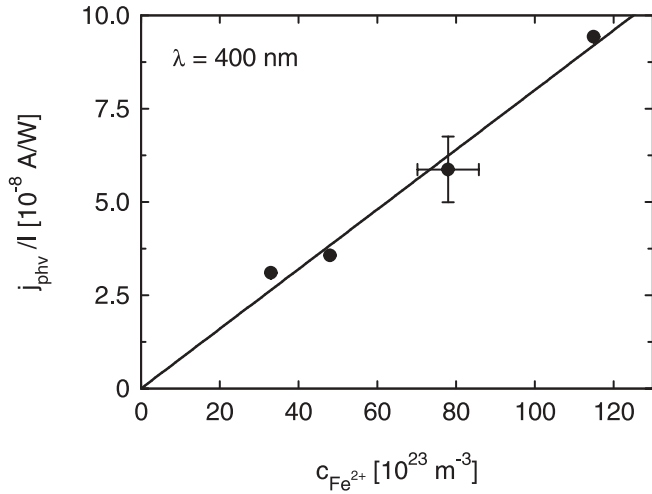
FIGURE 5   Specific photovoltaic current density j_{phv}/I in dependence on the concentration of Fe^{2+} ions. The *line* is a linear fit to the measured values
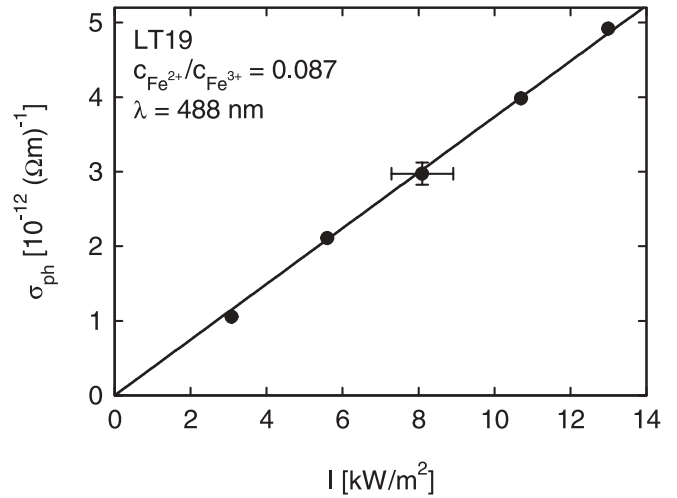

FIGURE 7   Photoconductivity σ_{ph} versus light intensity I. The *line* is a linear fit to the experimental data
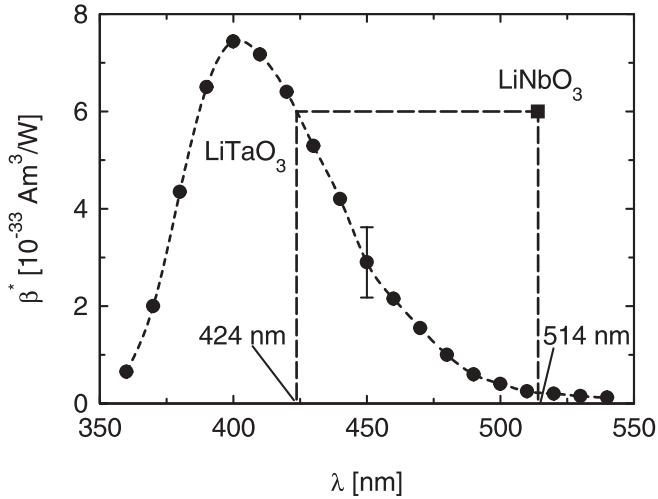

FIGURE 6   Spectral dependence of the specific photovoltaic coefficient β^*. The largest current density is measured at 400 nm. In $LiTaO_3$: Fe the value at about 420 nm is comparable with the value at 514 nm in $LiNbO_3$: Fe

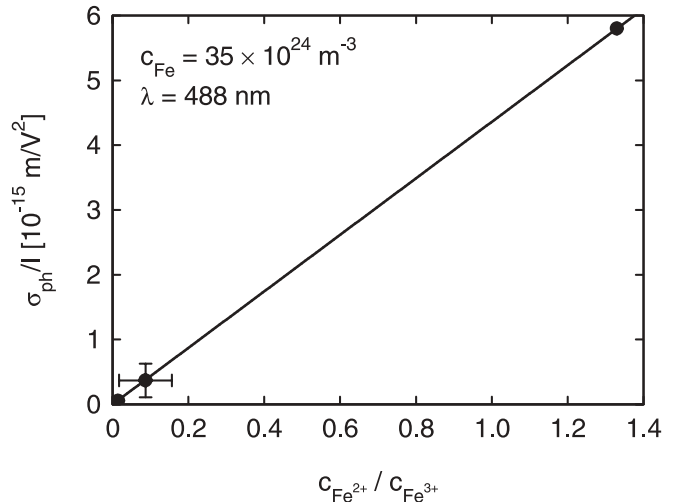**FIGURE 8**   Variation of the normalized photoconductivity σ_{ph}/I of a $LiTaO_3$: Fe crystal with the $c_{Fe^{2+}}/c_{Fe^{3+}}$ ratio. The *line* is a linear fit to the three measured values

The slope of the line in Fig. 5 corresponds to the specific photovoltaic coefficient β^* (2). In Fig. 6 the spectral dependence of β^* is plotted. The maximum of β^* is centered at 400 nm and for larger wavelengths than 400 nm β^* decreases. For shorter wavelengths than 400 nm β^* decreases rapidly. In comparison with $LiNbO_3$: Fe the curve $\beta^*(\lambda)$ is shifted to shorter wavelengths because in $LiNbO_3$: Fe the largest specific bulk photovoltaic coefficient β^* is achieved using blue light ($\lambda \approx 480$ nm).

4.4   *Photoconductivity*

During writing and erasing a hologram the time development of the refractive-index change Δn follows an exponential law with a time constant τ. The photoconductivity σ_{ph} can be determined from the time constant: $\sigma_{ph} = \varepsilon_{33}\varepsilon_0/\tau$. The photoconductivity σ_{ph} in $LiTaO_3$: Fe increases linearly with increasing light intensity (see Fig. 7). The normalized photoconductivity σ_{ph}/I is proportional to the $c_{Fe^{2+}}/c_{Fe^{3+}}$ concentration ratio. The slope of the line in Fig. 8 yields the spe-
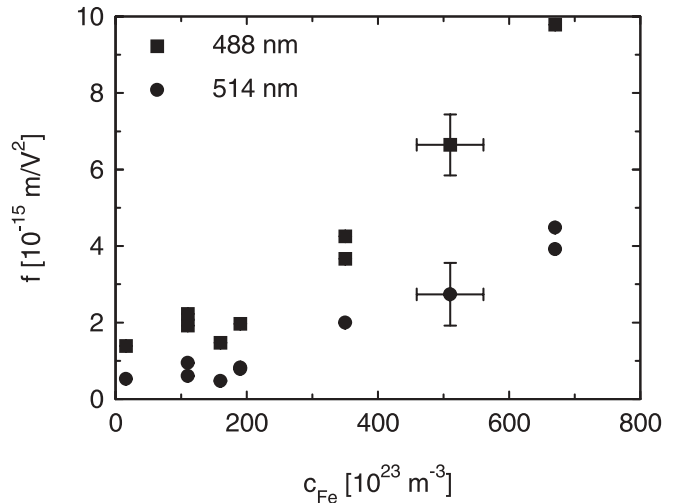

FIGURE 9   Specific photoconductivity $f = (\sigma_{ph}/I)/(c_{Fe^{2+}}/c_{Fe^{3+}})$ in dependence on the total amount of iron c_{Fe}. For small iron concentrations f is almost constant, but for larger concentrations ($c_{Fe} > 270 \times 10^{23}$ m^{-3}) the specific photoconductivity increases drastically
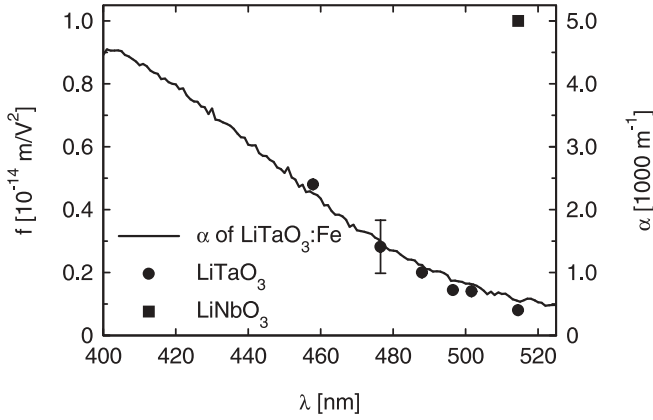
FIGURE 10 Spectral dependence of the specific photoconductivity f. The *solid curve* is the absorption coefficient α of the measured $LiTaO_3:Fe$ crystal

cific photoconductivity $f = (\sigma_{ph}/I)/(c_{Fe^{2+}}/c_{Fe^{3+}})$. The specific photoconductivity f is plotted in Fig. 9 versus the total iron concentration c_{Fe}. For small iron concentrations f is almost constant, but a remarkable increase of f can be observed if the iron concentration is larger than 270×10^{23} m^{-3}. The spectral dependence of the specific photoconductivity of a crystal with an iron concentration of 110×10^{23} m^{-3} can be seen in Fig. 10. Using light with a shorter wavelength yields a larger photoconductivity. The solid curve in Fig. 10 is the absorption coefficient α of the measured $LiTaO_3:Fe$ crystal. One can assume that f will reach a maximum at about 400 nm.

4.5 *Holographic sensitivity*

The holographic recording sensitivity S is calculated from the slope of the time development of the refractive-index change or the square root of the diffraction efficiency η, namely

$$S = \frac{1}{Id}\frac{\partial\sqrt{\eta}}{\partial t}\bigg|_{t=0}, \qquad (12)$$

with the light intensity I and the crystal thickness d. The sensitivity S increases with increasing Fe^{2+} concentration, as can be seen in Fig. 11.

4.6 *Dark conductivity*

The decay time τ_d of a hologram in the dark is measured in $LiNbO_3:Fe$ and $LiTaO_3:Fe$ at different temperatures T. If the crystals are not highly doped with iron the dark decay of Δn can be described with a single exponential function and the temperature dependence of τ_d follows an Arrhenius law (7). In Fig. 12 the variation of the dark storage times τ_d with temperature T of two $LiTaO_3:Fe$ and two $LiNbO_3:Fe$ crystals, both doped with 0.04 wt. % Fe, is presented. In all four crystals an activation energy of $E_A = 1.17 \pm 0.02$ eV is measured. At a given temperature the dark conductivities of the crystals depend on the proton concentrations that have been changed by thermal treatments. The concentrations can be estimated by the absorption coefficients $\alpha^o_{2870\,nm}$, which are 19 m^{-1} for the as-grown $LiTaO_3$, 196 m^{-1} for the proton-enriched $LiTaO_3$, 23 m^{-1} for the proton-reduced
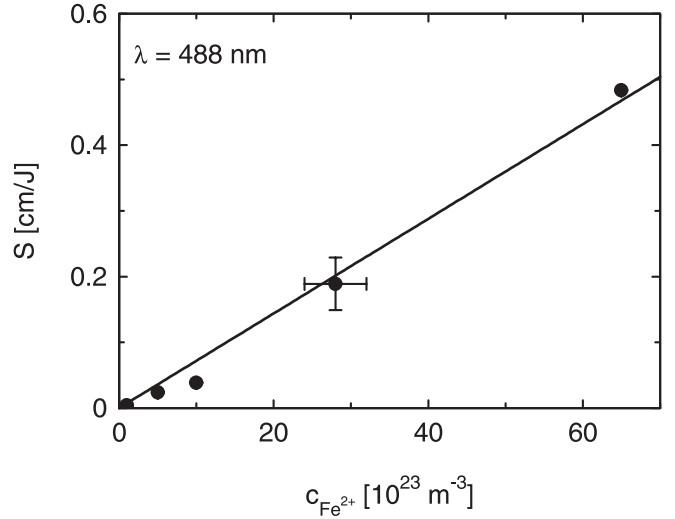

FIGURE 11 Holographic sensitivity S versus concentration of Fe^{2+}. The sensitivity for blue recording light increases linearly with increasing Fe^{2+} concentration
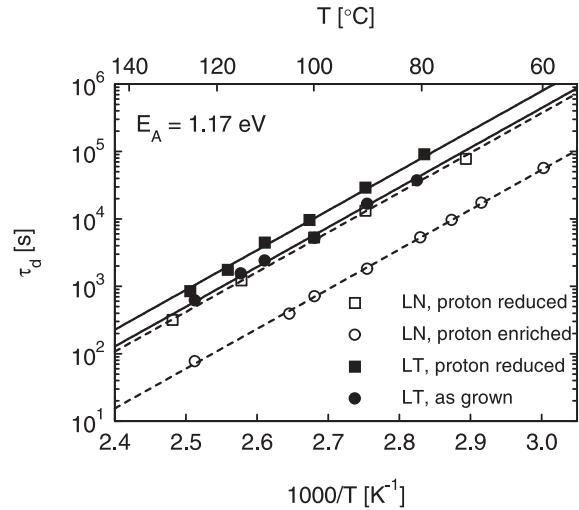

FIGURE 12 Variation of dark storage time τ_d with temperature T for two lithium niobate (LN) and two lithium tantalate (LT) crystals ($c_{Fe} \approx 0.04$ wt. %) with different proton concentrations. The *lines* are fits of the Arrhenius equation to the experimental data. The activation energy of the protons is the same in all crystals ($E_A = 1.17 \pm 0.02$ eV)

$LiNbO_3$, and 329 m^{-1} for the proton-enriched $LiNbO_3$. The as-grown $LiTaO_3$ crystal has an extrapolated dark storage time at room temperature of about 3.5 years and the proton-reduced $LiNbO_3$ crystal of about 1.7 years.

In highly doped $LiTaO_3:Fe$ crystals the dark storage time behaves completely differently. If the iron concentration is much larger than 350×10^{23} m^{-3}, the dark decay of a hologram is very fast. In the crystals 'LT20' and 'LT21' the dark storage time is of the order of hours. The process of the dark decay in highly doped $LiTaO_3$ is still under investigation.

5 Discussion

In congruently melting $LiTaO_3:Fe$ the experimental results can be explained in the framework of a charge-transport model with one photorefractive center ($Fe^{2+/3+}$) if the crystals are not highly doped with iron and if moder-

ate light intensities are used. The dependences of the photovoltaic current density, refractive-index change, photoconductivity, and sensitivity on the concentrations of Fe^{2+} and Fe^{3+} and on the light intensity are well described by the equations (2) to (5). At higher intensities shallow centers can also be populated with electrons, forming small polarons (Ta^{4+} at Li sites). The concentration of polarons increases with increasing intensity. Thus, the superlinear intensity dependence of j_{phv} can be explained by the contribution of polarons to the photovoltaic current density j_{phv}. However, at typical cw laser intensities the influence of polarons on the photovoltaic current density and on the refractive-index change is weak.

Differences from the predicted experimental dependences appear when the crystals are highly doped. The saturation value of the refractive-index change Δn_S increases linearly with increasing $c_{Fe^{3+}}$ concentration, but reaches a maximum of 3.5×10^{-4} at higher concentrations. This limitation is due to the specific photoconductivity f that also increases with increasing iron concentration c_{Fe}. According to the one-center model f should be constant. A larger photoconductivity could be explained with an increased mobility of electrons in the conduction band, but it is very doubtful that a larger concentration of defects leads to a higher mobility. Another reason for a higher photoconductivity might be a larger lifetime of electrons in the conduction band. This means that the capture cross section of the Fe^{3+} ions decreases with increasing c_{Fe} concentration. This might be possible because the Fe ions are normally incorporated at Li sites [21] and with increasing Fe concentrations some of the Fe ions could be placed at Ta sites. Fe ions at Li sites and Fe ions at Ta sites might have different capture cross sections. The last and most probable reason is that electrons can directly jump or tunnel between two neighboring Fe^{2+} and Fe^{3+} ions [4]. The distance between the iron ions is proportional to $c_{Fe}^{-1/3}$. It is experimentally verified that f increases exponentially with decreasing distance between the Fe ions if the iron concentration is larger than 270×10^{23} m^{-3}, as can bee seen in Fig. 13. Thus, a light-assisted tunneling or hopping of electrons between Fe ions becomes possible.

The maximum space-charge field that can be achieved in LiTaO$_3$: Fe can be calculated with the refractive index for red light ($\lambda = 633$ nm) $n_o = 2.177$, the electro-optic coefficient $r_{13} = 8.4$ pm/V, and the maximum refractive-index change 3.5×10^{-4}. The term $(n_o^3 r_{13})/2$, characteristic for the electro-optic effect (1), is 43 pm/V. Thus, the maximum refractive-index change of 3.5×10^{-4} corresponds to a space-charge field of $E_{SC} = 8.1$ kV/mm. The normalized refractive-index change $\Delta n_S / c_{Fe^{3+}}$ determined from holographic measurements (Fig. 3) can be compared with the measured values of the photoconductivity and the photovoltaic current density because the following equation applies: $\Delta n_S / c_{Fe^{3+}} = (n_o^3 r_{13} \beta^*)/(2f)$. With the measured values for green light ($\lambda = 514$ nm) $\beta^* = 2.4 \times 10^{-34}$ A m^3/W and $f = 6.8 \times 10^{-16}$ m/V^2 we get $\Delta n_S / c_{Fe^{3+}} = 1.5 \times 10^{-29}$ m^3. This fits very well to the measured value of 1.3×10^{-29} m^3 (see Table 3). The holographic sensitivity is proportional to the current density, i.e. proportional to j_{phv}, and therefore proportional to the $c_{Fe^{2+}}$ concentration.
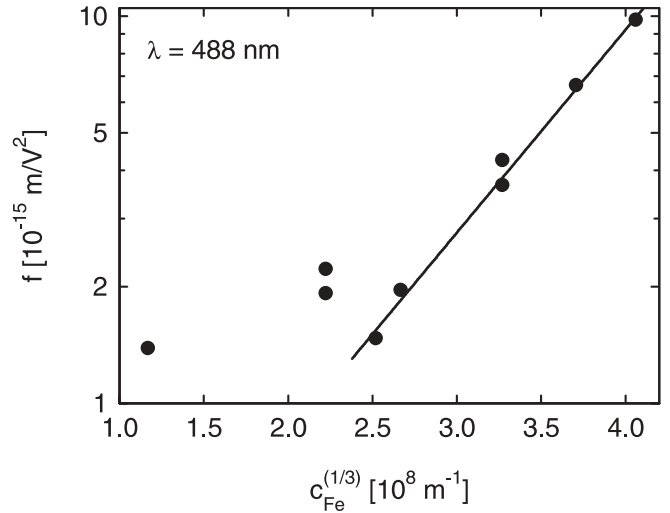

FIGURE 13 Logarithmic plot of the specific photoconductivity $f = (\sigma_{ph}/I)/(c_{Fe^{2+}}/c_{Fe^{3+}})$ of iron-doped LiTaO$_3$ at a wavelength of $\lambda = 488$ nm versus $c_{Fe}^{1/3}$ (see Fig. 9). The distance between the iron ions is inversely proportional to $c_{Fe}^{1/3}$. For small iron concentrations f is almost constant, but for larger concentrations ($c_{Fe} > 270 \times 10^{23}$ m^{-3}) the specific photoconductivity increases exponentially with decreasing distance (increasing $c_{Fe}^{1/3}$)

Parameter	LiTaO$_3$	LiNbO$_3$ [3]
$\Delta n_S/(mc_{Fe^{3+}})$ [m^3]	1.3×10^{-29}	3.0×10^{-29}
Δn_S^{max}	3.5×10^{-4}	6.2×10^{-4}
β^* @ 514 nm [Am^3/W]	2.4×10^{-34}	6.0×10^{-33}
β^* @ 400 nm [Am^3/W]	7.4×10^{-33}	–
f @ 514 nm [m/V^2]	6.8×10^{-16}	1.0×10^{-14}
f @ 400 nm [m/V^2]	$\sim 1.0 \times 10^{-14}$	–
$\mu_p/\mu_{p,LiNbO_3}$	~ 0.2	1

TABLE 3 Comparison of photorefractive properties of congruently melting iron-doped LiTaO$_3$ (this work) and LiNbO$_3$ [3]. We consider the specific refractive-index change ($c_{Fe} < 250 \times 10^{23}$ m^{-3}), the maximum refractive-index change Δn_S^{max} (read out with ordinarily polarized light, $\lambda = 633$ nm), the specific photovoltaic coefficient β_{31}^*, the specific photoconductivity f (4), and the ratio of the proton mobilities. The specific photoconductivity at 400 nm is estimated from the spectral dependence of f (Fig. 10)

The dark conductivity of LiTaO$_3$: Fe is mainly determined by the mobility and concentration of protons at a given temperature. The mobility μ_p increases exponentially with increasing temperature T and the activation energy of the protons is $E_A = 1.17$ eV. On the other hand, the dark decay of a hologram in highly doped ($c_{Fe} > 350 \times 10^{23}$ m^{-3}) crystals is very fast. The reason for this could also be direct transitions of electrons between Fe ions.

5.1   *Comparison of* LiTaO$_3$ *: Fe and* LiNbO$_3$ *: Fe*

In this work the photorefractive properties of LiTaO$_3$: Fe have been investigated to clarify whether LiTaO$_3$: Fe is an alternative to LiNbO$_3$: Fe concerning applications like holographic data storage. The photorefractive properties of LiNbO$_3$: Fe have been measured by several authors. Here, we compare the performance of LiTaO$_3$: Fe with values published by Peithmann et al. [3] because these authors have also examined highly doped LiNbO$_3$ crystals. A list of the main parameters of LiTaO$_3$: Fe and LiNbO$_3$: Fe is given in Table 3. We have determined the specific refractive-index

change ($c_{Fe} < 250 \times 10^{23}\,m^{-3}$), the maximum refractive-index change Δn_S^{max} for read out with ordinarily polarized red light ($\lambda = 633\,nm$), the specific photovoltaic coefficient β_{31}^*, the specific photoconductivity f (4), and the ratio of the proton mobilities. The specific photoconductivity of $LiTaO_3 : Fe$ at 400 nm is estimated from the spectral dependence of f (Fig. 10). In principle, $LiTaO_3 : Fe$ and $LiNbO_3 : Fe$ have similar properties and $LiTaO_3 : Fe$ also shows a limited dynamic range. The maximum space-charge field that can be achieved in $LiTaO_3 : Fe$ ($\approx 8.2\,kV/mm$) is only slightly smaller than the maximum field in $LiNbO_3$ ($\approx 9.5\,kV/mm$). Due to both, a smaller refractive index n_o and a smaller electro-optic coefficient r_{13} at $\lambda = 633\,nm$, the maximum refractive-index change of $LiTaO_3 : Fe$ is about 60% of that of $LiNbO_3 : Fe$. This should be different if ultraviolet light ($\lambda \approx 400\,nm$) is used for recording and reading holograms because here the refractive index ($n_o(400\,nm)^3/n_o(633\,nm)^3 = 1.15$) [22] and the electro-optic coefficient are larger. However, in the green spectral region $LiTaO_3 : Fe$ is less sensitive than $LiNbO_3 : Fe$ due to a smaller bulk photovoltaic coefficient and a smaller photoconductivity. In conclusion, one can assume that in $LiTaO_3 : Fe$ the values of the refractive-index change, holographic sensitivity, and photoconductivity at $\lambda \approx 400\,nm$ are comparable with the values of $LiNbO_3$ around 514 nm. As the proton mobility in $LiTaO_3$ is about five times smaller than the mobility in $LiNbO_3$, the dark storage time of holograms in $LiTaO_3$ exceeds that of $LiNbO_3$. Therefore, it should be interesting to examine the lifetime of thermally fixed holograms in $LiTaO_3$ because this lifetime is also limited by the proton conductivity.

6   Conclusions

Iron-doped $LiTaO_3$ crystals have been grown by the Czochralski method and their photorefractive properties were investigated with holographic methods. Properties like the refractive-index change, bulk photovoltaic current, holographic sensitivity, photoconductivity, and dark conductivity are very similar to those of $LiNbO_3 : Fe$. The main difference is the spectral dependence of the photoconductivity, photovoltaic current, and sensitivity because $LiTaO_3 : Fe$ is most sensitive around 400 nm and $LiNbO_3 : Fe$ at 480 nm. The main advantage of $LiTaO_3 : Fe$ is a larger dark storage time due to a smaller mobility of protons compared with that of $LiNbO_3 : Fe$. To optimize $LiTaO_3 : Fe$ for applications like long-term data storage, the correct iron and proton concentrations and the right wavelength of the recording light have to be chosen. The optimum iron concentration is $c_{Fe} \approx 300 \times 10^{23}\,m^{-3}$ and the crystal should be oxidized ($c_{Fe^{3+}} \approx c_{Fe}$) to achieve a large dynamic range. The dark storage time can be enhanced by reducing the proton concentration ($\alpha_{2870\,nm}^o < 20\,m^{-1}$), and the highest sensitivity is achieved using recording light at $\lambda \approx 400\,nm$.

REFERENCES

1 H.J. Coufal, D. Psaltis, G.T. Sincerbox: *Holographic Data Storage* (Springer, Berlin 2000)
2 P. Boffi, D. Piccinin, M.C. Ubaldi: *Infrared Holography for Optical Communications* (Springer, Berlin 2003)
3 K. Peithmann, A. Wiebrock, K. Buse: Appl. Phys. B **68**, 777 (1999)
4 I. Nee, M. Müller, K. Buse, E. Krätzig: J. Appl. Phys. **88**, 4282 (2000)
5 E. Krätzig, R. Orlowski: Appl. Phys. **15**, 133 (1978)
6 J. Imbrock, S. Wevering, K. Buse, E. Krätzig: J. Opt. Soc. Am. B **16**, 1392 (1999)
7 Y. Furukawa, K. Kitamura, S. Matsumura, P. Bernasconi, G. Montemezzani, P. Günter: in *Proc. Top. Meet. Photorefractive Materials, Effects and Devices, 1997* (OSA TOPS **27**) p. 153
8 S. Miyazawa, H. Iwasaki: Rev. Electr. Commun. Lab. **21**, 374 (1973)
9 J. Imbrock, D. Kip, E. Krätzig: Opt. Lett. **24**, 1302 (1999)
10 N.V. Kukhtarev, V.B. Markov, S.G. Odulov, M.S. Soskin, V.L. Vinetskii: Ferroelectrics **22**, 949 (1979)
11 A.M. Glass, D. von der Linde, T.J. Negran: Appl. Phys. Lett. **25**, 233 (1974)
12 E. Krätzig: Ferroelectrics **21**, 635 (1978)
13 R.G. Smith, D.B. Fraser, R.T. Denton, T.C. Rich: J. Appl. Phys. **39**, 4600 (1968)
14 Y.P. Yang, I. Nee, K. Buse, D. Psaltis: Appl. Phys. Lett. **78**, 4076 (2001)
15 D.L. Staebler, J.J. Amodei: Ferroelectrics **3**, 107 (1972)
16 S. Klauer, M. Wöhlecke, S. Kapphan: Phys. Rev. B **45**, 2786 (1992)
17 R.T. Smith, F.S. Welsh: J. Appl. Phys. **42**, 2219 (1971)
18 H. Kogelnik: Bell Syst. Tech. J. **48**, 2909 (1969)
19 Ch. Bäumer, D. Berben, K. Buse, H. Hesse, J. Imbrock: Appl. Phys. Lett. **82**, 2248 (2003)
20 Ch. Bäumer, C. David, A. Tunyagi, K. Betzler, H. Hesse, E. Krätzig, M. Wöhlecke: J. Appl. Phys. **93**, 3102 (2003)
21 H. Söthe, L.G. Rowan, J.-M. Spaeth: J. Phys.: Condens. Matter **1**, 3591 (1989)
22 K.S. Abedin, H. Ito: J. Appl. Phys. **80**, 6561 (1996)
23 D.S. Smith, H.D. Riccius, R.P. Edwin: Opt. Commun. **17**, 332 (1976)
24 K. Onuki, N. Uchida, T. Saku: J. Opt. Soc. Am. **62**, 1030 (1972)